◆ Human Brain Mapping 39:344–353 (2018) ◆

Accounting for the Role of Hematocrit in Between-Subject Variations of MRI-Derived Baseline Cerebral Hemodynamic Parameters and Functional BOLD Responses

Feng Xu,[1,2,3] Wenbo Li,[1,2] Peiying Liu,[1,2] Jun Hua,[1,2] John J. Strouse,[4] James J. Pekar,[1,2] Hanzhang Lu,[1,2] Peter C.M. van Zijl,[1,2] and Qin Qin [1,2]*

[1]*The Russell H. Morgan Department of Radiology and Radiological Science, Division of MR Research, Johns Hopkins University School of Medicine, Baltimore, Maryland*
[2]*F.M. Kirby Research Center for Functional Brain Imaging, Kennedy Krieger Institute, Baltimore, Maryland*
[3]*Developing Brain Research Lab, Children's National Medical Center, Washington DC, Washington*
[4]*Division of Hematology, Department of Medicine, Duke University, Durham, North Carolina*

Abstract: Baseline hematocrit fraction (Hct) is a determinant for baseline cerebral blood flow (CBF) and between-subject variation of Hct thus causes variation in task-based BOLD fMRI signal changes. We first verified in healthy volunteers ($n = 12$) that Hct values can be derived reliably from venous blood T_1 values by comparison with the conventional lab test. Together with CBF measured using phase-contrast MRI, this noninvasive estimation of Hct, instead of using a population-averaged Hct value, enabled more individual determination of oxygen delivery (DO_2), oxygen extraction fraction (OEF), and cerebral metabolic rate of oxygen ($CMRO_2$). The inverse correlation of CBF and Hct explained about 80% of between-subject variation of CBF in this relatively uniform cohort of subjects, as expected based on the regulation of DO_2 to maintain constant $CMRO_2$. Furthermore, we compared the relationships of visual task-evoked BOLD response with Hct and CBF. We showed that Hct and CBF contributed 22%–33% of variance in BOLD signal and removing the positive correlation with Hct and negative correlation with CBF allowed normalization of BOLD signal with 16%–22% lower variability. The results of this study suggest that adjustment for Hct effects is useful for studies of MRI perfusion and BOLD fMRI. *Hum Brain Mapp 39:344–353, 2018*.

Key words: MRI; Hct; CBF; DO_2; OEF; $CMRO_2$; BOLD

Contract grant sponsor: NIH; Contract grant number: K25 HL121192; Contract grant sponsor: American Society of Hematology; Contract grant number: Scholar Award; Contract grant sponsor: NIH; Contract grant number: P41 EB015909

Feng Xu and Wenbo Li contributed equally to this work.

*Correspondence to: Qin Qin, PhD; Department of Radiology, Johns Hopkins University School of Medicine, F.M. Kirby Research Center for Functional Brain Imaging, Kennedy Krieger Institute, 707 N. Broadway, Baltimore, MD 21205, USA. E-mail: qin@mri.jhu.edu

Received for publication 17 July 2017; Revised 22 September 2017; Accepted 4 October 2017.

DOI: 10.1002/hbm.23846
Published online 11 October 2017 in Wiley Online Library (wileyonlinelibrary.com).

INTRODUCTION

Magnetic resonance imaging (MRI) allows quantification of several baseline cerebral physiological parameters and the investigation of brain functional activity using blood-oxygenation-level-dependent (BOLD) signal changes. Understanding the physiological sources of between-subject variability is critical for the interpretation of these measures, especially for studies employing group comparison between healthy subjects and populations with various neurological or pathological conditions.

The hematocrit or proportion of whole blood that is red blood cells (Hct) governs an individual's oxygen (O_2) carrying capacity, and together with arterial oxygenation fraction (Y_a) and cerebral blood flow (CBF), determines the oxygen delivery (DO_2) to tissue.

$$DO_2 = [Hb_{tot}] \times Y_a \times CBF = C_{ery} \times Hct \times Y_a \times CBF \quad (1)$$

in which $[Hb_{tot}]$ is the total hemoglobin concentration in mM and $[Hb_{tot}] \times Y_a$ is the arterial oxygen content in μmol/mL. This can be determined from erythrocyte hemoglobin content, C_{ery}, which is the amount of the Hb monomer in a unit volume of fully oxygenated red blood cells. When taking a standardized mean corpuscular hemoglobin concentration or MCHC of 33.86 g/dL and a molecular mass of 16,125 g/mol for the monomer, C_{ery} equals 21.00 μmol Hb/mL or 21.00 μmol O_2/mL blood cells [Chanarin et al., 1984]. The oxygen concentration in arterial blood can then be obtained by multiplying C_{ery} with the Hct and Y_a.

Baseline activity of neuronal and glial cells is proportional to the cerebral metabolic rate of oxygen ($CMRO_2$). Owing to the requirement of a constant oxygen delivery to maintain a constant $CMRO_2$, any reduction in Hct leads to an increase in CBF and vice versa. This relationship has been well confirmed with positron emission tomography (PET) and single-photon emission computed tomography (SPECT), where this inverse correlation between Hct and CBF has been repeatedly observed, either by comparing between normal controls and patients with anemia or polycythemia [Brown et al., 1985; Henriksen et al., 2013; Herold et al., 1986; Ibaraki et al., 2010; Kuwabara et al., 2002; Prohovnik et al., 1989, 2009] or by examining within subjects before and after blood transfusion or hemodilution [Hino et al., 1992; Hudak et al., 1986; Massik et al., 1987; Metry et al., 1999; Vorstrup et al., 1992]. The requirement to maintain constant $CMRO_2$ through regulated DO_2 is described by the oxygen extraction fraction (OEF):

$$OEF = CMRO_2/DO_2 = (Y_a - Y_v)/Y_a \quad (2)$$

which is constant in healthy volunteers and generally stated in terms of a coupling between $CMRO_2$ and CBF. OEF was reported to show less variations than CBF among anemic patients with sickle cell disease [Herold et al., 1986] or chronic renal failure [Kuwabara et al., 2002; Metry et al., 1999].

In the MRI field, absolute CBF measurements using arterial spin labeling (ASL) techniques [Dai et al., 2008; Detre et al., 1992; Wong et al., 1998] are being standardized [Alsop et al., 2015]. Methods for OEF estimation have been introduced based on MR susceptometry [Fan et al., 2014; Fernandez-Seara et al., 2006; Haacke et al., 1997; Zhang et al., 2015] and T_2 relaxometry [Lu and Ge, 2008; Oja et al., 1999; Qin et al., 2011a; Wright et al., 1991]. Whole-brain $CMRO_2$ quantification by combining obtained CBF and OEF values has been done [Jain et al., 2010; Xu et al., 2009; Zhang et al., 2015]. Measurement of individual Hct values should allow more accurate estimation of DO_2 and $CMRO_2$. Furthermore, knowledge of Hct can help improve determination of OEF when using Hct-dependent susceptibility [Fan et al., 2014; Fernandez-Seara et al., 2006; Zhang et al., 2015] or T_2–Y_v calibration curves [Lu et al., 2012; Qin et al., 2011a].

The BOLD functional MRI (fMRI) signal reflects changes in cerebral blood volume (CBV), CBF, and $CMRO_2$ through complex biophysical mechanisms [Blockley et al., 2013; Hua et al., 2011; Kim and Ogawa, 2012; van Zijl et al., 1998, 2012]. The main cause of the effect is a temporary uncoupling of CBF and $CMRO_2$ [Blockley et al., 2013; Hua et al., 2011; Kim and Ogawa, 2012; van Zijl et al., 1998, 2012]. Positive correlation between Hct and BOLD amplitude has been observed in hemodilution experiments on anesthetized rats [Lin et al., 1998a,b] and in task-based fMRI studies on both healthy subjects [Gustard et al., 2003; Levin et al., 2001] and children with sickle cell anemia [Zou et al., 2011]. This is easy to understand because increased Hct causes a lower baseline CBF and thus a proportionally larger increase in BOLD signal change. Part of the interindividual variability of BOLD signal changes may therefore be due to between-subject variation of Hct. As such, incorporation of Hct measurement in MRI perfusion or functional protocols would allow adjustment for this global baseline factor. However, the conventional measure of Hct through laboratory analysis of a venous blood sample requires venipuncture, which may be painful and/or inconvenient for subjects in a research study.

Fortunately, the longitudinal relaxation time (T_1) of blood has a clear dependence on Hct, which is larger than on oxygenation [Brooks and Dichiro, 1987; Bryant et al., 1990; Grgac et al., 2013; Li et al., 2016a; Lu et al., 2004; Silvennoinen et al., 2003]. As blood T_1 values are important for MRI-based CBF quantification, fast MR sequences have been developed to obtain venous T_1 from large cerebral veins [Qin et al., 2011b; Varela et al., 2011; Wu et al., 2010]. Recently, we validated this technique with *in vitro* measurements and confirmed that blood T_1 values closely correlated with individual Hct [Li et al., 2016b]. The aim of this study is to demonstrate and verify that the Hct values converted from blood T_1 per subject can help improve MRI-based measurements of baseline DO_2, OEF, and $CMRO_2$, and account for the differences of CBF and BOLD effect among normal volunteers.

METHODS

All MR experiments were conducted on a 3.0 T MR System (Philips Healthcare, Best, The Netherlands) using a body coil for radiofrequency transmission and a 32-channel head coil for reception. Foam padding was used to stabilize the participant's head to minimize motion. A total of 13 healthy adults (35 ± 7 years old, 6 females and 7 males) were enrolled in this study and blood was sampled intravenously for complete blood count (CBC) immediately before or after the MRI scans. Each participant provided written informed consent and the study was approved by the Johns Hopkins Medicine Institutional Review Board.

MRI Experiments

The experiments and participants analyzed here were reported in a recent paper for measurement of arterial and venous blood T_1 values [Li et al., 2016b]; additional scans for venous blood T_2, global flow rates of the brain, and BOLD fMRI are reported in this study.

The protocols for obtaining arterial and venous blood T_1 values at ICA and IJV, respectively, have been described previously [Li et al., 2016b]. Acquiring the arterial T_1 from ICA requires extra repositioning of the subjects to have their chest covered by the body coil for complete inversion of the inflowing arterial blood [Li et al., 2016b]. Conversely, venous blood T_1 can be measured under the neuroimaging setup (centering at eye level). Thus, despite having an additional influence from oxygenation, obtaining venous blood T_1 is more straightforward for brain function studies. As an improvement to our earlier protocol for venous T_1 measurement at the IJV [Qin et al., 2011b], we replaced the segmented echo-planar imaging (EPI) acquisition with segmented turbo field echo (TFE) readout for better flow compensation [Li et al., 2016b]. The total acquisition time was 1 min.

To visualize the major neck vessels (ICA, internal carotid artery; VA, vertebral artery; IJV, internal jugular vein), a quick time-of-flight (TOF) angiogram was employed with parameters: TR/TE/flip angle (FA) = 26 ms/5.8 ms/20°, field of view (FOV) = 201 × 201 × 80 mm^3, nominal voxel size = 0.8 × 1.0 × 2.0 mm^3. A 60 mm saturation slab was positioned above the imaging slab to suppress the venous blood.

To acquire baseline whole-brain CBF, the blood flow rates at the bilateral ICA and VA were measured using phase-contrast (PC) MR angiography (MRA). PC MRA has been validated for quantitative flow measurements [Bakker et al., 1999; Evans et al., 1993; Zananiri et al., 1991]. Four runs of PC MRA were planned using a plane orientation perpendicular to the corresponding arteries as described previously [Liu et al., 2013b]: nominal voxel size = 0.5 × 0.5 × 5 mm^3, FOV = 200 × 200 × 5 mm^3, TR/TE/FA = 19 ms/9 ms/15°, maximum velocity encoding = 60 cm/s and 40 cm/s for ICA and VA, respectively, without cardiac triggering. Scan duration of each PC MRI scan was 20 s.

Additionally, a T_1-weighted magnetization-prepared rapid gradient-echo (MPRAGE) scan was added for brain volume estimation: TR/TE/FA = 12 ms/3.2 ms/9°, TI = 1,110 ms, FOV = 220 × 220 × 180 mm^3, nominal voxel size of 1.1 mm isotropic, SENSE factor = 2 × 2, duration of 5 min.

To obtain global OEF information, venous T_2 values were also measured at the IJV by employing a T2prep module with five separate effective echo times (eTE) of 20, 40, 80, 120, 160 ms. All the RF pulses used in the T2prep module were nonselective, to minimize sensitivity to flow. Composite refocusing pulses ($90°_x 180°_y 90°_x$) were applied with constant interecho spacing of 10 ms. The MR protocol followed an earlier study [Qin et al., 2011a] and the acquisition parameters were identical to the ones used for blood T_1 measurements, with 1 min acquisition time as well.

BOLD fMRI experiments used a radial yellow/blue-colored checkerboard flashing at 8 Hz. The visual paradigm had 30 s stimulation followed by 30 s of fixation on a cross-sign in the center of the screen, with four repetitions. An additional fixation period of 30 s was used at the beginning of the experiment. BOLD sequence parameters were as follows: TR/TE/FA = 2,000 ms/30 ms/70°; nominal voxel size 2.5 × 2.5 × 2.5 mm^3; SENSE factor = 2.1, 35 slices; FOV = 200 × 180 × 104 mm^3; with 136 dynamics.

Data Analysis

Matlab (MathWorks, Inc., Natick, MA) was used for data processing. Venous T_1 ($T_{1,v}$) was quantified following the fitting procedure described in Li et al. [2016b]. A linear fitting was performed between $1{,}000/T_{1,v}$ and Hct(lab), the Hct values provided by the CBC lab. Based on this calibration of Hct values from $T_{1,v}$, subsequent studies used $T_{1,v}$ to determine Hct, which we indicate as Hct($T_{1,v}$).

Analysis of PC MRI data followed methods used in previous studies [Liu et al., 2013b]. ROI of each of the four arteries was drawn manually on the magnitude image by tracing the boundaries of left and right ICAs and VAs. The velocity values calculated from the phase information within the mask were summed to yield the flux (in mL/min) of each artery. To account for brain size differences, the unit volume CBF (in mL/min/100 g) was obtained by normalizing the flux (in mL/min) of all four arteries to the parenchyma mass (in 100 g), which was estimated from the high-resolution T_1-weighted MPRAGE image using the software FSL (FMRIB software Library, Oxford University).

Assuming $Y_a = 0.98$, OEF was calculated as $OEF = 1 - Y_v/Y_a$. Based on previously reported Hct-dependent $T_{2,v}$–Y_v calibration curves [Lu et al., 2012], Y_v was determined from $T_{2,v}$ using either assumed Hct = 0.42 or Hct($T_{1,v}$).

Oxygen delivery was determined from Eq. (1) using $C_{ery} = 21.00$ μmol O_2/mL, $Y_a = 0.98$, and the Hct and CBF determined experimentally. $CMRO_2$ was calculated from

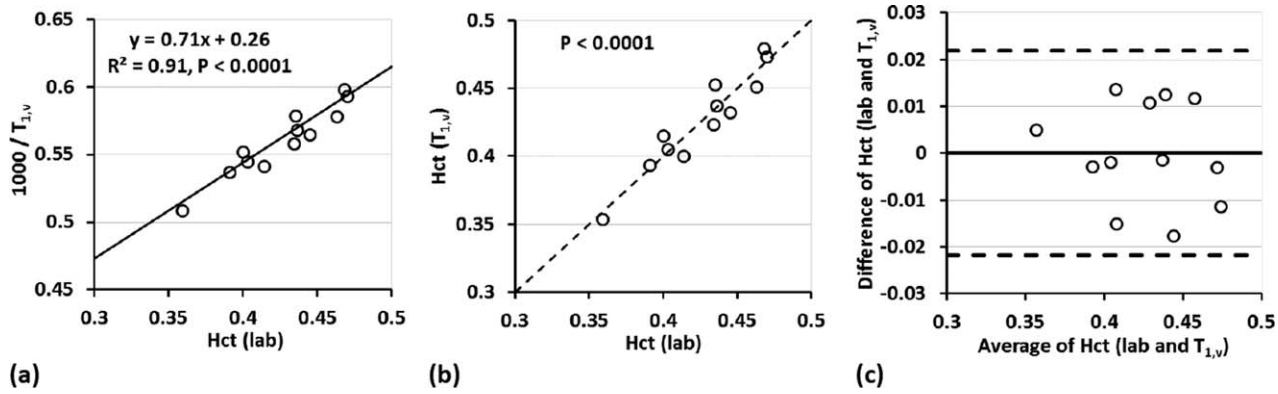

Figure 1.

(a) Scatter plot of the inverse of MR-measured venous blood T_1 and pathology lab measured Hct, Hct(lab). The fitted linear equation is used to determine Hct from the individual T_1 values. (b) Correlation plot of Hct(lab) and $T_{1,v}$-converted Hct, Hct($T_{1,v}$). The dashed line is the unity line. (c) Agreement (Bland–Altman plot) between Hct(lab) and Hct($T_{1,v}$). The horizontal solid line represents the mean difference of all subjects. The top and bottom dashed lines indicate two times the standard deviation from the mean difference.

DO_2 and OEF using Eq. (2). The units of DO_2 and $CMRO_2$ were μmol O_2/min/100 g.

Analysis of BOLD fMRI data was conducted using the software Statistical Parametric Mapping (SPM) (University College London, UK, version 5.0) and in-house MATLAB scripts. Dynamic BOLD fMRI time series were registered to the respective first volume to remove motion. Then all BOLD images were co-registered to the template of Montreal Neurological Institute (MNI) with a resampled voxel size of $2 \times 2 \times 2$ mm^3. Finally, the BOLD images were smoothed using a Gaussian filter with a full-width half-maximum (FWHM) of 8 mm. General linear analysis between voxel time course and stimulus paradigm convolved with an SPM-defined hemodynamic function was used to compute voxelwise T score comparing BOLD signal strength during visual stimulation with respect to that during epochs of visual fixation. Then T score was ranked from high to low. Visual activation was defined by the top 2,000 voxels within the occipital lobe (an approximation of visual cortex volume) on an individual basis. Time courses were averaged across these voxels. Percentage change of BOLD signal (S_{BOLD}) was given by linear regression of averaged time course with respect to the paradigm regressor.

Mean, standard deviation (STD), and coefficient of variation (CoV = STD/mean) across subjects were calculated for different physiological and functional parameters. Baseline CBF was investigated for a linear relationship with Hct($T_{1,v}$) by linear regression, $y = a \times x + b$. P values <0.05 were considered significant. The coefficient of determination, R^2, represents the percentage of the variance of one parameter explained by the variation of the other using a best-fit linear model. Adjusted R^2 was also calculated as

$$R^2_{adj} = 1-(1-R^2)\times(n-1)/(n-m-1) \quad (3)$$

This is to take into account the sample size (n) and number of variables (model complexity, m), and to correct the potential over-fitting issue caused by adding more regressors [Yin and Fan, 2001]. Although in this study we only performed linear regression with one variable ($m = 1$), the adjusted R^2 is intended to facilitate comparison with studies using multiple regressors.

Regression analyses of BOLD signal change were performed separately for its linear relationships ($y = a \times x + b$) with Hct and CBF. R^2, R^2_{adj}, and P values of the fitting were also calculated. Furthermore, covariate effects were removed by subtracting the fitted equation from the initial BOLD response to calculate the normalized BOLD response:

$$S_{BOLD,n} = S_{BOLD} - (a \times x + b) + \text{mean}(S_{BOLD}) \quad (4)$$

Equation (4) eliminates the dependence on both the slope (a) and the intercept of the fitted covariate model (b) [Liau and Liu, 2009]. It also preserves the mean of the BOLD signal changes for consistent comparison of CoV [Lu et al., 2010]. The residual correlation and the between-subject CoV of $S_{BOLD,n}$ after normalizing with different baseline parameters were evaluated.

RESULTS

The Hct values from the CBC tests and the venous T_1 values measured *in vivo* for all 13 subjects were previously reported [Li et al., 2016b]. Similar to the arterial blood T_1 values reported in the same paper [Li et al., 2016b], the

TABLE I. Summary of mean, standard deviation (STD), and coefficient of variance (CoV) of different parameters

					Y_v			DO_2 (μmol/min/100 g)		OEF		$CMRO_2$ (μmol/min/100 g)	
	$T_{1,v}$ (ms)	$T_{2,v}$ (ms)	Hct (lab)	Hct ($T_{1,v}$)	Hct = 0.42	Hct ($T_{1,v}$)	CBF (mL/min/100 g)	Hct = 0.42	Hct ($T_{1,v}$)	Hct = 0.42	Hct ($T_{1,v}$)	Hct = 0.42	Hct ($T_{1,v}$)
Mean	1,788	62.9	0.43	0.43	0.61	0.61	53.2	460.1	461.5	0.38	0.38	170.5	173.7
STD	83	11.8	0.034	0.036	0.058	0.048	9.4	81.1	47.8	0.059	0.049	21.1	19.5
CoV (%)	4.6	18.7	8.0	8.4	9.6	8.0	17.6	17.6	10.4	15.7	13.0	12.4	11.2

Y_v, DO_2, OEF, and $CMRO_2$ were calculated based on Hct = 0.42 and Hct($T_{1,v}$).

venous T_1 values correlated significantly with Hct (Fig. 1a) and the derived Hct values were calibrated as

$$\mathrm{Hct}(T_{1,v}) = \frac{1403}{T_{1,v}(\mathrm{ms})} - 0.36 \quad (5)$$

Linear regression (Fig. 1b) showed significant correlation ($P < 0.0001$) and Bland-Altman analysis (Fig. 1c) showed strong agreement between Hct(lab) and Hct($T_{1,v}$) ($n = 12$). We therefore from here on use only Hct($T_{1,v}$). Note that one subject was removed from this calibration as an outlier. The outlier detection was applied using the Grubbs criteria [Grubbs, 1950], which removes data with a difference more than 2 STD from the mean of the difference of Hct(lab) and Hct($T_{1,v}$). This outlier was rejected at the significance level of 0.05 (two-sided).

The group-averaged Hct($T_{1,v}$) values along with the baseline hemodynamic and metabolic parameters are listed in Table I. The CoV was 8.4% for Hct($T_{1,v}$) and 17.6% for CBF (Table I). The CoV for DO_2, OEF, and $CMRO_2$ derived from Hct($T_{1,v}$) were 10.4%, 13.0%, and 11.2%, which were very close to the numbers using Hct(lab) and lower than the values using an assumed population-averaged Hct of 0.42: 17.6% (CBF effect only), 15.7%, and 12.4% ($P < 0.05$, t test on subsamples).

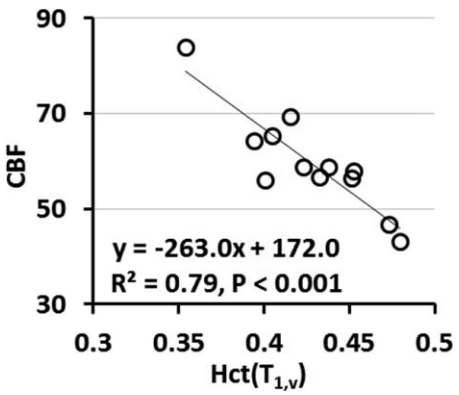

Figure 2.
Scatter plots of baseline CBF with Hct($T_{1,v}$). The linear regression is illustrated with a solid line. CBF shows inverse correlation with Hct values significantly ($P < 0.001$).

The significant inverse correlation of CBF with Hct($T_{1,v}$) ($P < 0.001$) is shown in Figure 2. The calculated R^2_{adj} value indicates that 77% of the between-subject variation of CBF can be explained by Hct (Table II).

The BOLD signal response showed positive correlation with Hct($T_{1,v}$), along with negative correlation with CBF ($P < 0.05$) (Fig. 3a,b). Based on the R^2_{adj} values, Hct alone explained 22% of the between-subject variation of S_{BOLD}, which was close to 33% for CBF (Table II). After eliminating the effects of Hct and CBF, respectively, the normalized BOLD responses, $S_{BOLD,n}$, displayed no correlation with these parameters (Fig. 3c,d). The CoV of S_{BOLD} was reduced by 16% and 22% (from 18.5% to 15.5% and 14.4%) after normalizing with Hct and CBF separately (Table III).

DISCUSSION

In this study, we adopted a recently developed fast sequence to quantify blood T_1 at IJV to estimate each individual's Hct. We investigated the correlation of Hct with baseline CBF and their relationship with BOLD signal, which were all obtained from the same session on healthy volunteers in completely noninvasive fashion. This study highlights three roles Hct plays in baseline perfusion and hemodynamics functional responses: (1) using individual Hct and CBF enabled more precise estimation of DO_2, OEF, and $CMRO_2$; (2) Hct explained about 80% of the between-subject variation of CBF (Table II and Fig. 2); (3) 22% of intersubject variability of BOLD response was associated with Hct (Table II and Fig. 3a) and normalization of BOLD with Hct reduced its CoV by 16% (Table III). The interrelations derived using blood T_1-converted Hct

TABLE II. Summary of the R^2 and R^2_{adj} for regression analysis of CBF values on Hct and BOLD signal changes on Hct and CBF

	CBF	S_{BOLD}	
	Hct($T_{1,v}$)	Hct($T_{1,v}$)	CBF
R^2	0.79	0.29	0.39
R^2_{adj}	0.77	0.22	0.33

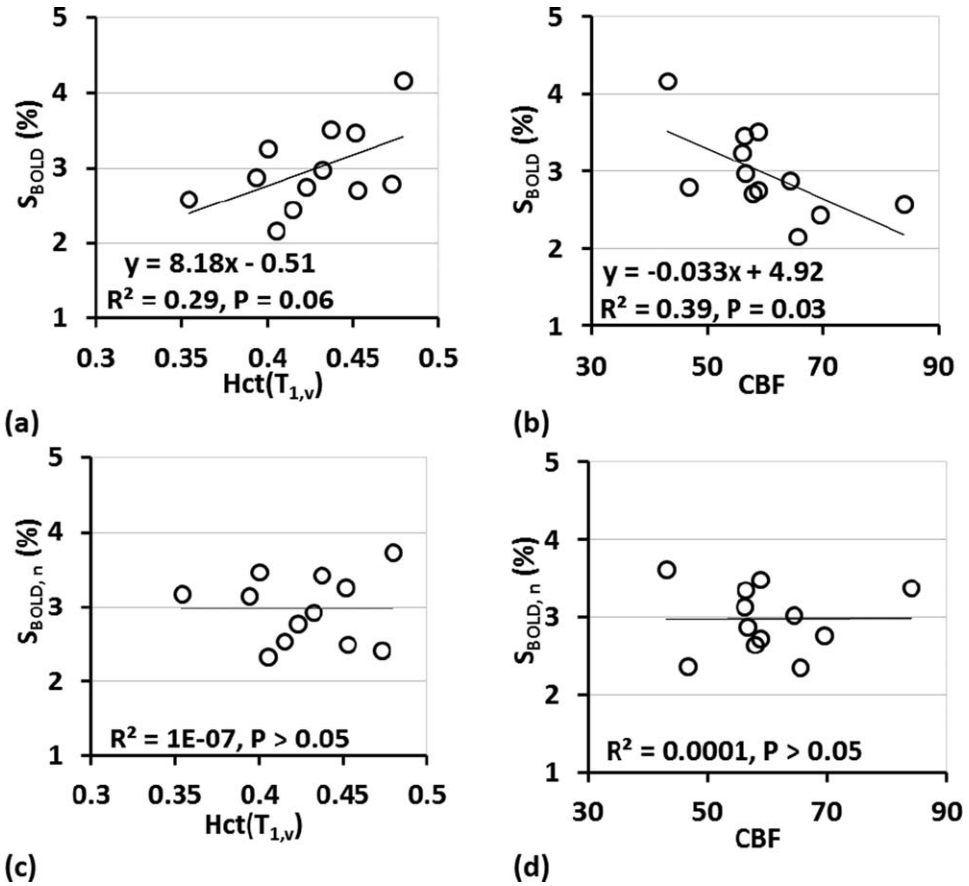

Figure 3.

Scatter plots of BOLD signal change (S_{BOLD}) with (a) Hct($T_{1,v}$) and (b) CBF. S_{BOLD} were positively correlated with (a) Hct ($P = 0.06$) and negatively correlated with (b) CBF ($P = 0.03$). (c,d) Scatter plots of normalized BOLD signal change ($S_{BOLD,n}$) after removing the variance explained by each effect [Eq. (4)].

information were consistent with those attained using lab test-based Hct values.

To prevent impairment of brain function, cerebral autoregulation relies on complex relationships between different hemodynamic and metabolic variables: CBF, CBV, DO_2, OEF, and $CMRO_2$ [Derdeyn et al., 2002; Ito et al., 2005]. Monitoring these parameters concurrently facilitates comprehensive examination of both oxygen supply and oxygen metabolism. During the last decade, the MRI field has seen growing interest in developing noninvasive techniques for quantifying physiologic variables beyond CBF [Ewing and Lu, 2013; Wong, 2013]. As observed in the present results, the between-subject CoV of DO_2, OEF, and $CMRO_2$ were only 56%–67% of CBF's CoV (10%–13% vs 18%, Table I). This reduced intersubject variability of DO_2, OEF, and $CMRO_2$ emphasizes their roles as more stable parameters in the presence of large physiological variation. Note that our measured CBF values have an inverse correlation with the measured OEF (data not shown), as expected based on Eqs. (1) and (2) and observed previously [Jain et al., 2010; Liu et al., 2013b; Peng et al., 2014; Xu et al., 2009]. Thus $CMRO_2$, as their product, is more constant across individuals, compared to these covarying parameters. Here we showed that by converting blood T_1 to Hct, more precise estimation of these parameters per-subject was made both directly (DO_2 and $CMRO_2$) and indirectly (OEF, through using a Hct-dependent $T_{2,v}-Y_v$ calibration model), compared to the typical practice of assuming the same Hct value for all subjects.

TABLE III. CoV of the BOLD and residual BOLD signal after removing the variance explained by Hct and CBF, respectively

	S_{BOLD}	$S_{BOLD,n}$: Hct($T_{1,v}$)	$S_{BOLD,n}$: CBF
Mean	2.98	2.97	2.98
STD	0.55	0.46	0.43
CoV (%)	18.5	15.5	14.4

In this study, ~80% between-subject CoV of CBF was associated with Hct (Table II and Fig. 2). To our best knowledge, this is the first MRI study on young healthy adults that confirmed previous understanding that between-subject variations of CBF can be partially explained by the variance in Hct [Brown et al., 1985; Henriksen et al., 2013; Herold et al., 1986; Ibaraki et al., 2010; Kuwabara et al., 2002; Prohovnik et al., 1989, 2009]. Such a highly significant correlation between CBF and Hct was also found in an early report including subjects with both normal hematology and various blood disorders [Brown et al., 1985]. Our results indicate that, at least for the young healthy subjects recruited in this work, Hct is the primary determinant of the variability of CBF. Sex is often considered to be a covariate for CBF, which is largely due to the Hct difference between females and males [Henriksen et al., 2013; Ibaraki et al., 2010] (36% ~ 44% vs 41% ~ 50%) [Chanarin et al., 1984].

CBF is known to be affected by many other factors, such as arterial partial pressure of carbon dioxide ($PaCO_2$), cardiac function, age, caffeine, smoking status, alcohol, psychiatric state, cardiovascular diseases, and pharmaceutical drugs [Giardino et al., 2007; Henriksen et al., 2013; Ibaraki et al., 2010; Ito et al., 2005; Lu et al., 2011; van der Veen et al., 2015]. In a recent study examining factors affecting global CBF among a relatively healthy elderly group, 14% of between-subject CBF variation is explained by Hct, along with 17% by end-tidal PCO_2 ($P_{ET}CO_2$), 11% by caffeine, and 10% by homocysteine [Henriksen et al., 2014]. This much reduced effect of Hct to CBF variation is perhaps largely due to the difference of age (mean age [range] = 35 [27–51] years old vs 64 [50–75] years old) and sample size ($n = 12$ vs 38) between the two studies. It is expected that a range of additional factors other than Hct may contribute to CBF variability among an aged group compared to a younger population. For group-comparison studies, taking into account individual Hct could help disentangle the multiple covariates influencing the obtained CBF values.

Our inspection showed that the R^2 values of the correlation between BOLD signal change for 8 Hz checkerboard visual activation and Hct($T_{1,v}$) and CBF were 0.29 and 0.39 (Table II and Fig. 3a,b). Previous task-evoked functional studies reported R^2 values for correlation between BOLD and Hct as 0.23 [Gustard et al., 2003] and 0.28 [Levin et al., 2001], and R^2 values for correlation between BOLD and CBF as 0.17 [Lu et al., 2008] and 0.46 [Liau and Liu, 2009]. The high correlation between Hct and baseline CBF as discussed above elucidates the overlapping origin of these two regressors for BOLD response. These fitted correlation not only illustrate various sources of the variability for BOLD signal but also were useful for the normalization of the S_{BOLD} to lower its CoV [Eq. (4), Table III, and Fig. 3c,d]. The reduction of between-subject CoV of $S_{BOLD,n}$ is desired for enhancing the detection power in the group-level comparisons [Liau and Liu, 2009; Liu et al., 2013a,c; Lu et al., 2010].

A few notes of the methodology of this study need to be commented upon. First, the measured venous T_1 values are dependent on both Hct and Y_v [Brooks and Dichiro, 1987; Bryant et al., 1990; Grgac et al., 2013; Li et al., 2016a; Lu et al., 2004; Silvennoinen et al., 2003]. Except during ischemia, arterial T_1 is only affected by Hct as Y_a is close to 1, thus is in theory a better surrogate for Hct estimation. Comparing to measuring arterial T_1 values, measuring venous T_1 values is relatively straightforward. Our data suggested that venous T_1 values are also largely modulated by Hct among normal volunteers and Hct values derived from $T_{1,v}$ show high correlation and agreement with lab measured Hct (Fig. 1). When Y_v values of the populations under investigation have large variations, arterial blood T_1 is suggested for more accurate Hct estimation using a previously developed conversion formula [Li et al., 2016b]. Note that several methods were developed to rapidly measure venous T_1 in vivo, all of which used a Look-Locker scheme but with various acquisition modules: segmented balanced steady-state free precession, bSSFP [Wu et al., 2010]; single-shot EPI [Varela et al., 2011]; segmented EPI [Qin et al., 2011b]; and segmented TFE [Li et al., 2016b]. The reported average $T_{1,v}$ values for healthy females and males agree well: 1,831/1,746 ms [Li et al., 2016b], 1,779/1,662 ms [Varela et al., 2011], and 1,827/1,677 ms [Wu et al., 2010]. Based on our calibration formula [Eq. (5)], ±5% error of $T_{1,v}$ measurement would cause 9%–10% underestimation or overestimation of Hct, respectively. Thus, the Hct method does not depend critically on the sequence used.

Second, this work obtained global CBF using PC MRA instead of regional CBF using ASL. Compared to ASL, PC MRA is a faster approach for estimating global flow rate with simpler methodology for both acquisition and analysis. In contrast, ASL can provide local perfusion values. It is expected that regional differences in the correlation between baseline CBF and Hct may exist, due to the relationship between CBF and local neuronal activity. ASL can be technically challenging and has low signal sensitivity. Additionally, ASL is sensitive to blood T_1 [Alsop et al., 2015] and CBF values could be underestimated using overestimated blood T_1. A recent study in a large population reported significant correlation between these two methods [Dolui et al., 2016]. More variance in CBF values estimated with PC MRA was reported and may be related to inaccurate placement of a single imaging plane through all arteries of interest [Dolui et al., 2016]. Note that nongated PC MRA scans were performed in our study for estimating global CBF values. Additionally, the dynamic variation of arterial lumen area over the cardiac cycle was not considered. Changes in lumen area of up to 27% have been reported between diastolic and systolic phases in common carotid arteries [Chow et al., 2008]. Nonetheless, the effect of cardiac pulsation might be canceled out by signal averaging during the 20 s PC MRA scans. Earlier work from small groups of subjects did not find significant difference

of averaged velocity from PC MRA with or without cardiac gating [Qin et al., 2011b; Xu et al., 2009].

Third, one limitation of our visual stimuli-evoked BOLD experiments is that no MR-compatible vision-correction lenses were provided for subjects with myopia, which resulted in additional subject-dependent variations into the BOLD signal [Lu et al., 2010]. This may have increased the interindividual variation in BOLD signals reported in this study.

Last, we did not separate the between-subject variations of each MRI outcome from the within-subject variations or measurement noise of the techniques used. This is usually determined by repeated measures on each subject. Recently we reported that the intrasession, intersession, and intersubject CoV of obtained arterial blood T_1 values were 1.1%, 2.1%, and 5.6%, respectively [Li et al., 2016b]. A previous study using the same PC MRA protocol for CBF estimation showed its intrasession, intersession, and intersubject CoV to be 2.8%, 7.4%, and 17.4%, respectively [Liu et al., 2013b]. CoV of BOLD signal reproducibility for the visual task was 14% depending on the extent of spatial smoothing applied [Raemaekers et al., 2012].

Although Hct effects have been separately analyzed in various studies of CBF, DO_2, OEF, $CMRO_2$, and functional BOLD as aforementioned, this work sought to revisit and emphasize its importance in adopting a more multiparametric and integral approach in MRI field. As blood T_1 itself is an important parameter for quantifying CBF using ASL [Alsop et al., 2015] and CBV change using vascular space occupancy (VASO) techniques [Lu et al., 2003], Hct measures from blood T_1 values will prove to be an effective noninvasive approach assisting perfusion and functional MRI studies, at least for healthy volunteers. The calibrated Hct$-T_{1,v}$ relation [Eq. (5)] is not expected to be valid for patients with different hemoglobin (e.g., sickled blood or fetal blood). Recent advances in multiwavelength pulse oximetry permit estimation of total hemoglobin or Hct using a percutaneous sensor [Barker and Badal, 2008; Lindner and Exadaktylos, 2013]. The accuracy of this technique has been evaluated in different clinical settings and promising results have been demonstrated [Frasca et al., 2011; Lindner and Exadaktylos, 2013]. Our internal comparison with CBC lab test on both healthy volunteers and those with anemia found lack of accuracy for a subgroup (data not shown). Once further improved and validated, a handheld pulse oximeter would be an ideal point of care device for both Hct and Y_a determination for a broad population.

CONCLUSION

We utilized a recently developed MR technique to quickly (1 min) and noninvasively (no blood draw) estimate Hct values in normal volunteers. This allowed more convenient and precise per-subject determination of physiological parameters that characterize oxygen delivery, extraction, and consumption in the brain. The close correlation of Hct with baseline CBF and task-based BOLD signal changes indicates that Hct may play an important role in explaining interindividual variance of baseline CBF and thus BOLD signal responses. In addition, we showed that BOLD signal normalized with Hct had less variability than original BOLD signal. These findings are pertinent to a wide range of MRI-based brain perfusion and function studies.

REFERENCES

Alsop DC, Detre JA, Golay X, Gunther M, Hendrikse J, Hernandez-Garcia L, Lu H, MacIntosh BJ, Parkes LM, Smits M, van Osch MJ, Wang DJ, Wong EC, Zaharchuk G (2015): Recommended implementation of arterial spin-labeled perfusion MRI for clinical applications: A consensus of the ISMRM perfusion study group and the European consortium for ASL in dementia. Magn Reson Med 73:102–116.

Bakker CJ, Hoogeveen RM, Viergever MA (1999): Construction of a protocol for measuring blood flow by two-dimensional phase-contrast MRA. J Magn Reson Imag 9:119–127.

Barker SJ, Badal JJ (2008): The measurement of dyshemoglobins and total hemoglobin by pulse oximetry. Curr Opin Anaesthesiol 21:805–810.

Blockley NP, Griffeth VE, Simon AB, Buxton RB (2013): A review of calibrated blood oxygenation level-dependent (BOLD) methods for the measurement of task-induced changes in brain oxygen metabolism. NMR Biomed 26:987–1003.

Brooks RA, Dichiro G (1987): Magnetic-resonance-imaging of stationary blood - A review. Med Phys 14:903–913.

Brown MM, Wade JP, Marshall J (1985): Fundamental importance of arterial oxygen content in the regulation of cerebral blood flow in man. Brain 108: 81–93.

Bryant RG, Marill K, Blackmore C, Francis C (1990): Magnetic-relaxation in blood and blood-clots. Magn Reson Med 13: 133–144.

Chanarin I, Brozovic M, Tidmarsh E, Waters D (1984): Blood and Its Disease. New York: Churchill Livingstone.

Chow TY, Cheung JS, Wu Y, Guo H, Chan KC, Hui ES, Wu EX (2008): Measurement of common carotid artery lumen dynamics during the cardiac cycle using magnetic resonance TrueFISP cine imaging. J Magn Reson Imag 28:1527–1532.

Dai W, Garcia D, de Bazelaire C, Alsop DC (2008): Continuous flow-driven inversion for arterial spin labeling using pulsed radio frequency and gradient fields. Magn Reson Med 60: 1488–1497.

Derdeyn CP, Videen TO, Yundt KD, Fritsch SM, Carpenter DA, Grubb RL, Powers WJ (2002): Variability of cerebral blood volume and oxygen extraction: Stages of cerebral haemodynamic impairment revisited. Brain 125:595–607.

Detre JA, Leigh JS, Williams DS, Koretsky AP (1992): Perfusion imaging. Magn Reson Med 23:37–45.

Dolui S, Wang Z, Wang DJ, Mattay R, Finkel M, Elliott M, Desiderio L, Inglis B, Mueller B, Stafford RB, Launer LJ, Jacobs DR, Jr., Bryan RN, Detre JA (2016): Comparison of noninvasive MRI measurements of cerebral blood flow in a large multisite cohort. J Cereb Blood Flow Metab 36:1244–1256.

Evans AJ, Iwai F, Grist TA, Sostman HD, Hedlund LW, Spritzer CE, Negro-Vilar R, Beam CA, Pelc NJ (1993): Magnetic resonance

imaging of blood flow with a phase subtraction technique. In vitro and in vivo validation. Invest Radiol 28:109–115.
Ewing J, Lu H (2013): MRI measures of cerebral physiology. NMR Biomed 26:885–886.
Fan AP, Bilgic B, Gagnon L, Witzel T, Bhat H, Rosen BR, Adalsteinsson E (2014): Quantitative oxygenation venography from MRI phase. Magn Reson Med 72:149–159.
Fernandez-Seara MA, Techawiboonwong A, Detre JA, Wehrli FW (2006): MR susceptometry for measuring global brain oxygen extraction. Magn Reson Med 55:967–973.
Frasca D, Dahyot-Fizelier C, Catherine K, Levrat Q, Debaene B, Mimoz O (2011): Accuracy of a continuous noninvasive hemoglobin monitor in intensive care unit patients. Crit Care Med 39:2277–2282.
Giardino ND, Friedman SD, Dager SR (2007): Anxiety, respiration, and cerebral blood flow: Implications for functional brain imaging. Compr Psychiatry 48:103–112.
Grgac K, van Zijl PC, Qin Q (2013): Hematocrit and oxygenation dependence of blood (1)H(2)O T(1) at 7 Tesla. Magn Reson Med 70:1153–1159.
Grubbs FE (1950): Sample criteria for testing outlying observations. Ann Math Stat 21:27–58.
Gustard S, Williams EJ, Hall LD, Pickard JD, Carpenter TA (2003): Influence of baseline hematocrit on between-subject BOLD signal change using gradient echo and asymmetric spin echo EPI. Magn Reson Imag 21:599–607.
Haacke EM, Lai S, Reichenbach JR, Kuppusamy K, Hoogenraad FG, Takeichi H, Lin W (1997): In vivo measurement of blood oxygen saturation using magnetic resonance imaging: A direct validation of the blood oxygen level-dependent concept in functional brain imaging. Hum Brain Mapp 5:341–346.
Henriksen OM, Jensen LT, Krabbe K, Guldberg P, Teerlink T, Rostrup E (2014): Resting brain perfusion and selected vascular risk factors in healthy elderly subjects. PLoS One 9:e97363.
Henriksen OM, Kruuse C, Olesen J, Jensen LT, Larsson HB, Birk S, Hansen JM, Wienecke T, Rostrup E (2013): Sources of variability of resting cerebral blood flow in healthy subjects: A study using (1)(3)(3)Xe SPECT measurements. J Cereb Blood Flow Metab 33:787–792.
Herold S, Brozovic M, Gibbs J, Lammertsma AA, Leenders KL, Carr D, Fleming JS, Jones T (1986): Measurement of regional cerebral blood flow, blood volume and oxygen metabolism in patients with sickle cell disease using positron emission tomography. Stroke 17:692–698.
Hino A, Ueda S, Mizukawa N, Imahori Y, Tenjin H (1992): Effect of hemodilution on cerebral hemodynamics and oxygen metabolism. Stroke 23:423–426.
Hua J, Stevens RD, Huang AJ, Pekar JJ, van Zijl PC (2011): Physiological origin for the BOLD poststimulus undershoot in human brain: Vascular compliance versus oxygen metabolism. J Cereb Blood Flow Metab 31:1599–1611.
Hudak ML, Koehler RC, Rosenberg AA, Traystman RJ, Jones MD Jr (1986): Effect of hematocrit on cerebral blood flow. Am J Physiol 251:H63–H70.
Ibaraki M, Shinohara Y, Nakamura K, Miura S, Kinoshita F, Kinoshita T (2010): Interindividual variations of cerebral blood flow, oxygen delivery, and metabolism in relation to hemoglobin concentration measured by positron emission tomography in humans. J Cereb Blood Flow Metab 30:1296–1305.
Ito H, Kanno I, Fukuda H (2005): Human cerebral circulation: Positron emission tomography studies. Ann Nucl Med 19: 65–74.
Jain V, Langham MC, Wehrli FW (2010): MRI estimation of global brain oxygen consumption rate. J Cereb Blood Flow Metab 30: 1598–1607.
Kim SG, Ogawa S (2012): Biophysical and physiological origins of blood oxygenation level-dependent fMRI signals. J Cereb Blood Flow Metab 32:1188–1206.
Kuwabara Y, Sasaki M, Hirakata H, Koga H, Nakagawa M, Chen T, Kaneko K, Masuda K, Fujishima M (2002): Cerebral blood flow and vasodilatory capacity in anemia secondary to chronic renal failure. Kidney Int 61:564–569.
Levin JM, Frederick Bde B, Ross MH, Fox JF, von Rosenberg HL, Kaufman MJ, Lange N, Mendelson JH, Cohen BM, Renshaw PF (2001): Influence of baseline hematocrit and hemodilution on BOLD fMRI activation. Magn Reson Imag 19:1055–1062.
Li W, Grgac K, Huang A, Yadav N, Qin Q, van Zijl PC (2016a): Quantitative theory for the longitudinal relaxation time of blood water. Magn Reson Med 76:270–281.
Li W, Liu P, Lu H, Strouse JJ, van Zijl PC, Qin Q (2016b): Fast measurement of blood T1 in the human carotid artery at 3T: Accuracy, precision, and reproducibility. Magn Reson Med Epub Ahead of Print.
Liau J, Liu TT (2009): Inter-subject variability in hypercapnic normalization of the BOLD fMRI response. NeuroImage 45: 420–430.
Lin W, Paczynski RP, Celik A, Hsu CY, Powers WJ (1998a): Effects of acute normovolemic hemodilution on T2*-weighted images of rat brain. Magn Reson Med 40:857–864.
Lin W, Paczynski RP, Celik A, Hsu CY, Powers WJ (1998b): Experimental hypoxemic hypoxia: Effects of variation in hematocrit on magnetic resonance T2*-weighted brain images. J Cereb Blood Flow Metab 18:1018–1021.
Lindner G, Exadaktylos AK (2013): How noninvasive haemoglobin measurement with pulse co-oximetry can change your practice: An expert review. Emerg Med Int 2013:701529.
Liu P, Hebrank AC, Rodrigue KM, Kennedy KM, Park DC, Lu H (2013a): A comparison of physiologic modulators of fMRI signals. Hum Brain Mapp 34:2078–2088.
Liu P, Xu F, Lu H (2013b): Test-retest reproducibility of a rapid method to measure brain oxygen metabolism. Magn Reson Med 69:675–681.
Liu TT, Glover GH, Mueller BA, Greve DN, Brown GG (2013c): An introduction to normalization and calibration methods in functional MRI. Psychometrika 78:308–321.
Lu H, Clingman C, Golay X, van Zijl PCM (2004): Determining the longitudinal relaxation time (T1) of blood at 3.0 Tesla. Magn Reson Med 52:679–682.
Lu H, Golay X, Pekar JJ, van Zijl PCM (2003): Functional magnetic resonance Imaging based on changes in vascular space occupancy. Magn Reson Med 50:263–274.
Lu H, Xu F, Grgac K, Liu P, Qin Q, van Zijl P (2012): Calibration and validation of TRUST MRI for the estimation of cerebral blood oxygenation. Magn Reson Med 67:42–49.
Lu H, Xu F, Rodrigue KM, Kennedy KM, Cheng Y, Flicker B, Hebrank AC, Uh J, Park DC (2011): Alterations in cerebral metabolic rate and blood supply across the adult lifespan. Cereb. Cortex 21:1426–1434.
Lu H, Yezhuvath US, Xiao G (2010): Improving fMRI sensitivity by normalization of basal physiologic state. Hum Brain Mapp 31:80–87.
Lu HZ, Ge YL (2008): Quantitative evaluation of oxygenation in venous vessels using T2-relaxation-under-spin-tagging MRI. Magn Reson Med 60:357–363.

Lu HZ, Zhao CG, Ge YL, Lewis-Amezcua K (2008): Baseline blood oxygenation modulates response amplitude: Physiologic basis for intersubject variations in functional MRI signals. Magn Reson Med 60:364–372.

Massik J, Tang YL, Hudak ML, Koehler RC, Traystman RJ, Jones MD Jr (1987): Effect of hematocrit on cerebral blood flow with induced polycythemia. J Appl Physiol 62:1090–1096.

Metry G, Wikstrom B, Valind S, Sandhagen B, Linde T, Beshara S, Langstrom B, Danielson BG (1999): Effect of normalization of hematocrit on brain circulation and metabolism in hemodialysis patients. J Am Soc Nephrol 10:854–863.

Oja JME, Gillen JS, Kauppinen RA, Kraut M, van Zijl PCM (1999): Determination of oxygen extraction ratios by magnetic resonance imaging. J Cereb Blood Flow Metab 19: 1289–1295.

Peng SL, Dumas JA, Park DC, Liu P, Filbey FM, McAdams CJ, Pinkham AE, Adinoff B, Zhang R, Lu H (2014): Age-related increase of resting metabolic rate in the human brain. NeuroImage 98:176–183.

Prohovnik I, Hurlet-Jensen A, Adams R, De Vivo D, Pavlakis SG (2009): Hemodynamic etiology of elevated flow velocity and stroke in sickle-cell disease. J Cereb Blood Flow Metab 29: 803–810.

Prohovnik I, Pavlakis SG, Piomelli S, Bello J, Mohr JP, Hilal S, De Vivo DC (1989): Cerebral hyperemia, stroke, and transfusion in sickle cell disease. Neurology 39:344–348.

Qin Q, Grgac K, van Zijl PC (2011a): Determination of whole-brain oxygen extraction fractions by fast measurement of blood T(2) in the jugular vein. Magn Reson Med 65: 471–479.

Qin Q, Strouse JJ, van Zijl PC (2011b): Fast measurement of blood T(1) in the human jugular vein at 3 Tesla. Magn Reson Med 65:1297–1304.

Raemaekers M, du Plessis S, Ramsey NF, Weusten JM, Vink M (2012): Test-retest variability underlying fMRI measurements. NeuroImage 60:717–727.

Silvennoinen MJ, Kettunen MI, Kauppinen RA (2003): Effects of hematocrit and oxygen saturation level on blood spin-lattice relaxation. Magn Reson Med 49:568–571.

van der Veen PH, Muller M, Vincken KL, Westerink J, Mali WP, van der Graaf Y, Geerlings MI, Group SS (2015): Hemoglobin, hematocrit, and changes in cerebral blood flow: The second manifestations of arterial disease-magnetic resonance study. Neurobiol Aging 36:1417–1423.

van Zijl PC, Hua J, Lu H (2012): The BOLD post-stimulus undershoot, one of the most debated issues in fMRI. NeuroImage 62: 1092–1102.

van Zijl PCM, Eleff SM, Ulatowski JA, Oja JME, Ulug AM, Traystman RJ, Kauppinen RA (1998): Quantitative assessment of blood flow, blood volume and blood oxygenation effects in functional magnetic resonance imaging. Nat Med 4:159–167.

Varela M, Hajnal JV, Petersen ET, Golay X, Merchant N, Larkman DJ (2011): A method for rapid in vivo measurement of blood T1. NMR Biomed 24:80–88.

Vorstrup S, Lass P, Waldemar G, Brandi L, Schmidt JF, Johnsen A, Paulson OB (1992): Increased cerebral blood flow in anemic patients on long-term hemodialytic treatment. J Cereb Blood Flow Metab 12:745–749.

Wong EC (2013): New developments in arterial spin labeling pulse sequences. NMR Biomed 26:887–891.

Wong EC, Buxton RB, Frank LR (1998): Quantitative imaging of perfusion using a single subtraction (QUIPSS and QUIPSS II). Magn Reson Med 39:702–708.

Wright GA, Hu BS, Macovski A (1991): Estimating oxygen-saturation of blood in vivo with MR imaging at 1.5T. J Magn Reson Imag 1:275–283.

Wu WC, Jain V, Li C, Giannetta M, Hurt H, Wehrli FW, Wang J (2010): In vivo venous blood T1 measurement using inversion recovery true-FISP in children and adults. Magn Reson Med 64:1140–1147.

Xu F, Ge YL, Lu HZ (2009): Noninvasive quantification of whole-brain cerebral metabolic rate of oxygen ($CMRO_2$) by MRI. Magn Reson Med 62:141–148.

Yin P, Fan X (2001): Estimating R^2 shrinkage in multiple regression: A comparison of different analytical methods. J Exp Educ 69:203–224.

Zananiri FV, Jackson PC, Goddard PR, Davies ER, Wells PN (1991): An evaluation of the accuracy of flow measurements using magnetic resonance imaging (MRI). J Med Eng Technol 15:170–176.

Zhang J, Liu T, Gupta A, Spincemaille P, Nguyen TD, Wang Y (2015): Quantitative mapping of cerebral metabolic rate of oxygen (CMRO2) using quantitative susceptibility mapping (QSM). Magn Reson Med 74:945–952.

Zou P, Helton KJ, Smeltzer M, Li CS, Conklin HM, Gajjar A, Wang WC, Ware RE, Ogg RJ (2011): Hemodynamic responses to visual stimulation in children with sickle cell anemia. Brain Imag Behav 5:295–306.